buildings

MDPI

Article

Tests and Seismic Response Analysis of Guided-Rail-Type Anti-Tensile Rubber Bearing

Longfei Zhang [1,2,*], Xiang Lan [1,2], Kechuan Wu [1,2] and Wenzheng Yu [1,2]

[1] College of Architecture and Civil Engineering, Kunming University, Kunming 650214, China; lx523947015@kmu.edu.cn (X.L.); wukc@kmu.edu.cn (K.W.); yuwenzheng@kmu.edu.cn (W.Y.)
[2] Institute of Engineering Earthquake Resistance and Disaster Reduction, Kunming University, Kunming 650214, China
* Correspondence: zhanglongfei08052003@kmu.edu.cn

Abstract: When subjected to seismic activity, tall isolated buildings with a high aspect ratio are susceptible to overturning as a result of the failure of rubber isolation bearings under tension. In order to address this issue, a guided-rail tension device (GR) has been developed to enhance the tensile strength of rubber bearings. Furthermore, a novel guided-rail isolation rubber bearing (GR&RB) has been proposed as a potential solution. Quasi-static tests have been conducted to investigate the mechanical properties of the GR, as well as the GR&LNR600 and LNR600. Additionally, numerical finite element analysis has been employed to study the seismic response of the GR&RB under El Centro seismic action in a high-rise building with an aspect ratio of approximately 4. The experimental results suggest that the inclusion of GRs has a limited effect on the horizontal mechanical attributes of rubber isolation bearings. Nevertheless, it simultaneously enhances their tensile strength, demonstrating a significant augmentation of 4.23 times. Moreover, the mechanical behavior of the GR aligns with the Hook model. The numerical analysis suggests that the utilization of GR&RB can mitigate the tensile stress levels of rubber isolators. Furthermore, it is recommended to augment the elastic tensile stiffness of the GR while reducing the open value to enhance the tensile efficiency, with the potential to attain up to 75% efficiency in tensile performance.

Keywords: seismic isolation; tensile rubber isolation bearings; guided-rail tension device; experimental study; finite element analysis

check for updates

Citation: Zhang, L.; Lan, X.; Wu, K.; Yu, W. Tests and Seismic Response Analysis of Guided-Rail-Type Anti-Tensile Rubber Bearing. *Buildings* **2024**, *14*, 992. https://doi.org/10.3390/buildings14040992

Academic Editors: Hiroshi Tagawa, Xinghuai Huang and Yeshou Xu

Received: 14 February 2024
Revised: 26 March 2024
Accepted: 30 March 2024
Published: 3 April 2024

Copyright: © 2024 by the authors. Licensee MDPI, Basel, Switzerland. This article is an open access article distributed under the terms and conditions of the Creative Commons Attribution (CC BY) license (https://creativecommons.org/licenses/by/4.0/).

1. Introduction

Base isolation is a widely utilized and effective technique to mitigate vibrations in mid-rise and low-rise buildings, demonstrating favorable seismic performance [1–4].

As research in isolation technology progresses, new avenues of investigation have emerged. In an effort to enhance the seismic resilience of buildings situated in mountainous regions, Zhang et al. [5] introduced an isolated step-terrace structure and conducted shaking table experiments on a 1:10 scale model of this innovative system. The outcomes revealed that the seismic performance of the isolated step-terrace structure significantly surpassed that of conventional step-terrace configurations. Rayegani et al. [6,7] explored the phenomenon of seismic pounding resulting from the excessive deformation of the isolation layer during near-fault earthquakes. Their study introduced the use of magnetorheological dampers within the isolation layer, which proved effective in mitigating displacement and preventing pounding occurrences. Furthermore, they assessed the seismic collapse probability and life cycle cost associated with the implementation of smart hybrid isolation structures in the presence of pounding effects. Zelleke et al. [8] introduced a reliability-based multi-hazard optimization framework tailored to base-isolated buildings subjected to diverse multi-hazard scenarios. Tena-Colunga et al. [9] conducted a study on four independent slender steel structure buildings in sturdy soil, finding that the seismic

responses of slender base-isolated structures can be significantly compromised during strong earthquakes.

With the increasing endorsement of base isolation technology by relevant authorities in China, its application has expanded to encompass high-rise buildings, such as the Kunming Tianhu Jingxiu, a notable high-rise shear wall renovation project [10]. To prevent the potential damage to rubber bearings resulting from tension, which could lead to the overturning of isolated structures, it is imperative that isolators do not experience tensile stress. Even in cases where tensile stress does occur, it should be maintained below 1.0 MPa in accordance with Chinese seismic regulations [11,12]. However, in the context of high-rise buildings with high aspect ratios, the manifestation of the overturning effect under seismic action is conspicuous, often resulting in tensile stress in isolators. Numerous studies have indicated the limited tensile resistance of rubber isolators [13,14]. When subjected to tension, the rubber bearing may develop internal cavities due to negative pressure [15], despite exhibiting no external signs of damage, consequently leading to a reduction in vertical compressive stiffness to approximately half of the isolator's initial stiffness. Moreover, when the tensile stress reaches 1.5–3.0 MPa, the tensile stiffness of the rubber isolator undergoes a sharp decline, signifying complete damage to the rubber bearing [16]. Consequently, the issue of tensile failure in rubber isolators has consistently impeded the widespread application of seismic isolation technology in high-rise buildings [17].

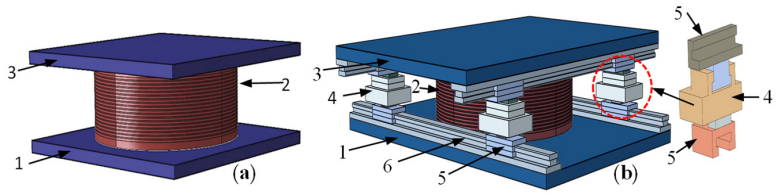
Many scholars have conducted extensive research to address the challenge of tensile failure in rubber isolators. Kelly et al. [18] applied a ball-and-socket joint linkage system to resist the tensile forces in the isolation system. Nagarajaiah et al. [19] proposed a combination of springs and rubber isolators to enhance the tensile performance and recentering capability of rubber isolators. Kasalanti et al. [20] employed the prestress technique to prevent the tensile failure of isolators. Qi et al. [21] recommended the addition of vertical steel bars at the edges of isolators to enhance their tensile safety. Yan et al. [22] developed three types of three-dimensional base isolators by serially connecting horizontal isolation sub-devices with vertical isolation sub-devices to counteract overturning. Su et al. [23] proposed the parallel connection of three laminated rubber isolators to convert tension into compression. Wang et al. [24] introduced tension-laminated rubber bearings (TLRB) with a specified tensile capacity and provided calculation formulas for their horizontal stiffness in compression and tension states, as well as a formula to calculate the limit shear strain of the bearings. Ge et al. [25] established design criteria for the tensile performance of rubber isolators through tensile–shear tests and developed a gate-shaped device for tension. Pauletta et al. [26] investigated the impact of the vulcanization time and the rubber formulation process on the tensile characteristics of rubber bearings by conducting tensile experiments on prototype rubber bearings. The study put forth recommendations aimed at enhancing the tensile properties of rubber bearings. Zhang et al. [27] delved into the tensile behavior of thick rubber bearings (TRBs) via numerical simulations and analytical examinations. Their work presented an analytical framework tailored to represent the tensile behavior of the bearings under cyclic loading conditions. However, many of these devices or methods that enhance the tensile capacity of rubber isolators may concurrently diminish their horizontal isolation performance, resulting in a reduction in the horizontal isolation efficiency of the base isolation structure and constraining their application in engineering.

It should be noted that Vaiana et al. [28] categorized rubber bearings into two primary groups, steel-reinforced elastomeric bearings (SREBs) and fiber-reinforced elastomeric bearings (FREBs), distinguished by their reinforcement methods. SREBs incorporate steel shims for reinforcement, while FREBs utilize fibers, offering cost-effectiveness advantages in production and installation. By default, the rubber bearings discussed in this paper are specifically steel-reinforced elastomeric bearings (SREBs), denoted as RB. In light of the aforementioned challenges, this paper proposes a guided-rail tension device (GR) to augment the tensile strength of rubber isolators. Additionally, a novel guided-rail isolation rubber bearing (GR&RB) is introduced for high-rise buildings with high aspect ratios. The horizontal and vertical mechanical properties of the GR are examined through pseudo-static

tests, and the dynamic response of the GR&RB under earthquake action is investigated using numerical methods in high-rise isolated structures with a high aspect ratio.

2. Structure of GR&RB

In general, the RB configuration typically consists of an upper attachment plate, a rubber bearing, and a lower attachment plate, with the rubber bearing situated between the upper and lower attachment plates and typically connected to them using bolts. As depicted in Figure 1a, under tension, the interaction between the upper and lower attachment plates and the internal rubber layer of the rubber bearing can generate a negative pressure void. This phenomenon weakens the lateral constraint of the steel plate on the internal rubber layer, resulting in a significant reduction in the vertical compressive stiffness of the rubber bearings and consequently impacting the overall safety of the isolated structure.



Note: 1—Lower attachment plate, 2—Rubber bearing, 3—Upper attachment plate, 4—Tension device, 5—T-shaped fasteners, 6—Guide rail.

Figure 1. Structures of isolators: (**a**) RB; (**b**) GR&RB.

In an effort to enhance the tensile performance, guided-rail tension devices (GRs) are integrated with RBs to form a guided-rail isolation rubber bearing (GR&RB), as illustrated in Figure 1b. The GR&RB system comprises a lower attachment plate, a rubber bearing, four guide rails, four tension devices, T-shaped fasteners, and an upper attachment plate. The rubber bearing and tension devices are positioned between the upper and lower attachment plates and are connected to them using bolts. Each tension device is equipped with T-shaped fasteners on both ends, which are designed to interact with the guide rails. The guide rails are attached to the upper and lower connecting plates using bolts. When the upper and lower attachment plates undergo horizontal relative deformation, the T-shaped fasteners can freely slide along the guide rails, facilitating the coordination of the tension devices with the horizontal deformation of the rubber bearings. Under tension in the upper and lower attachment plates, the tension devices, through their interaction with the guide rails, share the tensile load with the rubber bearing, thereby reducing the tensile effect on the rubber bearing and preventing the generation of negative pressure voids between the internal rubber layer and the steel plate. Conversely, when the rubber bearing is under compression, the tension devices do not bear any pressure, as the entirety of the pressure is supported by the rubber bearing.

3. Experimental Tests

The uniaxial tensile limit characteristics of a single GR were examined, as well as the properties of the GR&LNR600 (a specific GR&RB configuration where the rubber bearing is LNR600) and LNR600. The findings from these tests were subsequently utilized in the dynamic analysis of a high-rise isolated structure. It is worth noting that in the uniaxial ultimate tensile test of a single GR, the length of the GR was limited to 600 mm, which was shorter than the GR length used in the GR&LNR600 configuration.

3.1. Test Specimens

All GRs utilized in the experiment were constructed from carbon structural steel (referred to as No. 45 in GB). The specific parameters of the LNR600 employed in the GR&LNR600 configuration are detailed in Table 1, while the primary dimensions of the GR&LNR600 system are visually represented in Figure 2.

Table 1. Details of LNR600.

Outer diameter	D (mm)	600
Inner diameter	d (mm)	100
Total height	H (mm)	263
Rubber layer thickness	t_r (mm)	6.22
Number of rubber layers	n_r	18
Total thickness of rubber layers	T_r (mm)	112
Steel shim thickness	ts (mm)	3
Number of steel shims	n_s	17
Total thickness of steel shims	T_s (mm)	51
Primary shape factor	S_1	23.44
Secondary shape factor	S_2	5.35

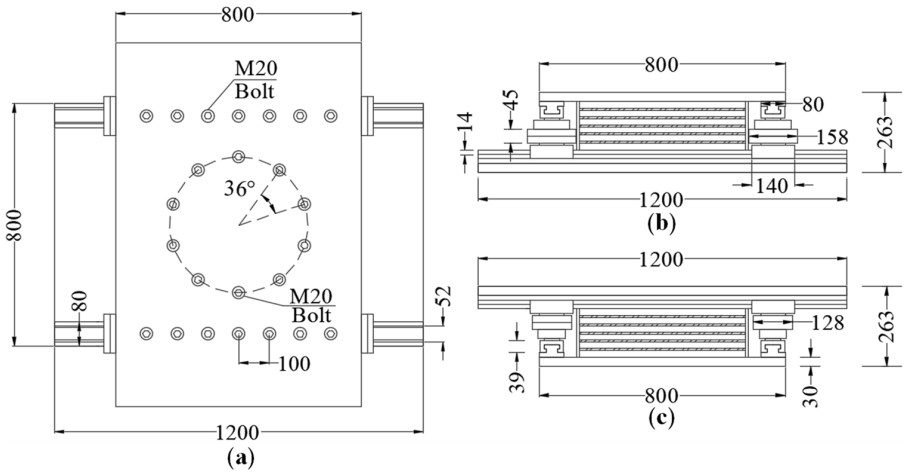


Figure 2. Main dimensions of GR&LNR600 (**a**) vertical view; (**b**) front view; (**c**) left view. Unit: mm.

3.2. Test Equipment

The mechanical performance tests of the LNR600 and GR&LNR600 were conducted on a shear testing device (see Figure 3a), and the uniaxial ultimate tensile test for a single GR was performed on an electro-hydraulic servo testing device (see Figure 3b). Both sets of testing equipment contained a self-balanced system.

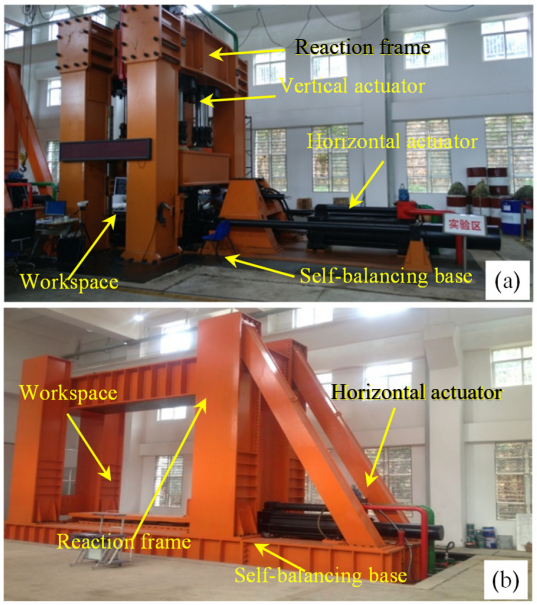


Figure 3. Test equipment: (**a**) shear testing device; (**b**) electro-hydraulic servo testing device.

3.3. Test Procedure

The uniaxial tensile tests of the single GR, LNR600, and GR&LNR600 were carried out under displacement-controlled loading, employing a loading rate of 1 mm/s. Notably, the single GR was subjected to failure under tension, whereas the tensile displacements of the LNR600 and GR&LNR600 were limited to 5.2 mm to ensure specimen elasticity.

To examine the impact of the angle between the horizontal shear direction and the guide rail on the mechanical properties of the guided-rail isolation rubber bearings, loading angles of 45° and 0° were considered in the horizontal compression–shear and tensile–shear cyclic tests of the GR&LNR600, as presented in Table 2. The LNR600 utilized in tests T1 to T6 represented the same natural rubber bearing, with Figure 4 illustrating the loading directions for these tests. The shear tests of the LNR600 and GR&LNR600 were conducted in accordance with the industry standard within the Chinese construction sector [29]. Furthermore, the horizontal equivalent stiffness (K_b) of rubber isolation bearings was derived from a quasi-static test consisting of 3 cycles at a loading frequency of 0.02 Hz and a 100% shear strain amplitude.

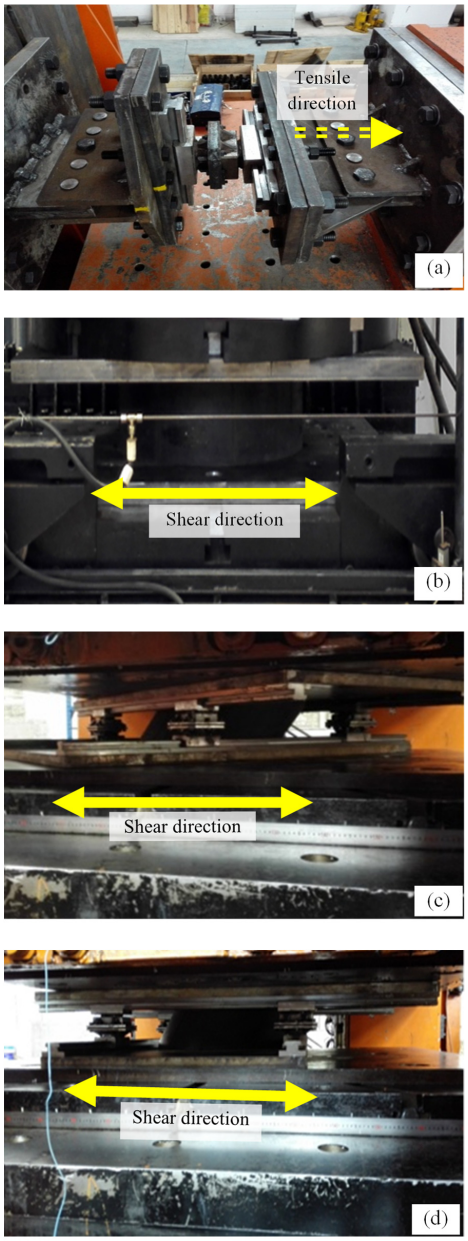


Figure 4. Loading direction: (**a**) single GR; (**b**) LNR600; (**c**) GR&LNR600-45°; (**d**) GR&LNR600-0°.

Table 2. Shear test scheme.

Test Item	Test No.	Subject	Horizontal Loading Angle	Vertical Load
Compression–shear	T1	LNR600	/	Pressure loads of 4239 kN
	T2	GR&LNR600	45°	
	T3	GR&LNR600	0°	
Tensile–shear	T4	LNR600	/	Tensile loads of 282.6 kN
	T5	GR&LNR600	45°	
	T6	GR&LNR600	0°	

3.4. Test Results

3.4.1. Tensile Properties

During the initial phase of the single GR tensile failure test, no visible deformation was observed in the guide rail. As the loading displacement increased, the GR experienced sudden failure, leading to the separation of the central connecting component. Simultaneously, the damaged section on the left slid down onto the test platform, and the middle section of the guide rail underwent bending under tension, as depicted in Figure 5. The tensile force–displacement curve of the GR uniaxial tension is illustrated in Figure 6.

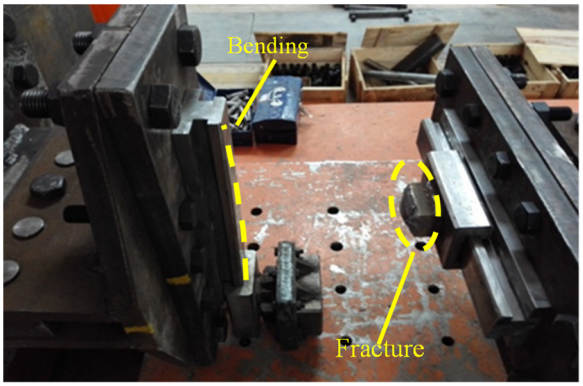


Figure 5. Single GR tensile failure.

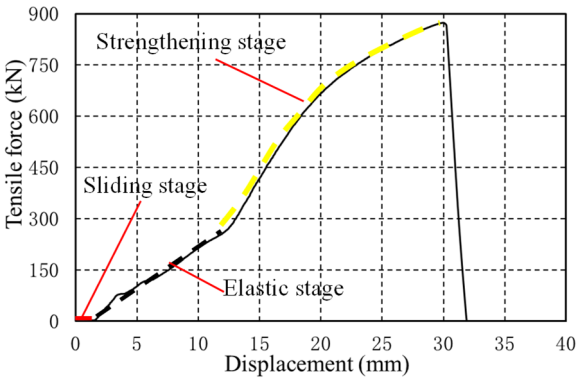


Figure 6. Tensile force–displacement curve of GR uniaxial tension.

The analysis of the tensile force–displacement curve reveals three distinct stages in the tensile process of the GR: the slip stage, elastic stage, and strengthening stage. The slip stage is attributed to the clearance between GR components, which is linked to the processing accuracy, with a gap value of 1.4 mm. Upon reaching tensile displacement of 30.1 mm, the GR specimen experiences sudden failure, leading to a sharp drop in load. Assuming the ultimate tensile bearing capacity of the GR corresponds to the end of the elastic stage, the design bearing capacity of a single GR is estimated to be 266 kN, with elastic tensile

stiffness of 27.6 kN/mm and a gap value of 1.4 mm. The tensile behavior of the GR can be described as the Hook model, as depicted in Figure 7, and can be expressed as

$$f = \begin{cases} k(d-l) & (if \quad d-l > 0) \\ 0 & (otherwise) \end{cases} \tag{1}$$

where k is the elastic tensile stiffness of the GR, d is the axial deformation value of the GR, and l is the gap value ($l \geq 0$).

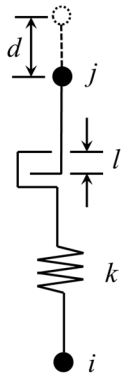


Figure 7. Diagram of Hook model.

Figure 8 presents the load–displacement curves of the GR&LNR600 and LNR600 in the uniaxial tensile tests. The tensile bearing capacity of the GR&LNR600 reached 1195 kN, approximately 4.23 times that of the LNR600, indicating a significant enhancement in the tensile performance of the conventional rubber isolation bearings due to the GRs.

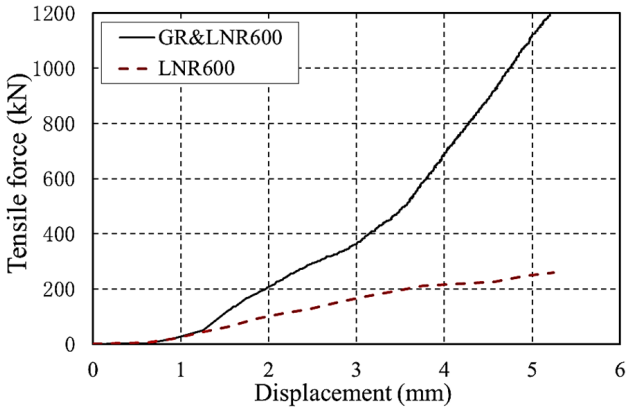


Figure 8. Tensile force–displacement curves of GR&LNR600 and LNR600.

3.4.2. Horizontal Compression–Shear and Tensile–Shear Performance

For ease of reference, the tensile bearings with angles of 45° and 0° between the horizontal loading direction and the guide rail are denoted as GR&LNR600-45° and GR&LNR600-45°, respectively. According to JG/T 118-2018 [29], the horizontal equivalent stiffness K_b is defined as the slope of the hysteretic curve between −100% and +100% shear deformation with reference to the third cycle of the test. Figure 9 illustrates the hysteresis curves of the horizontal compressive–shear and tensile–shear tests for specimens T1 to T6. The measured horizontal equivalent stiffness values of each specimen are summarized in Table 3.

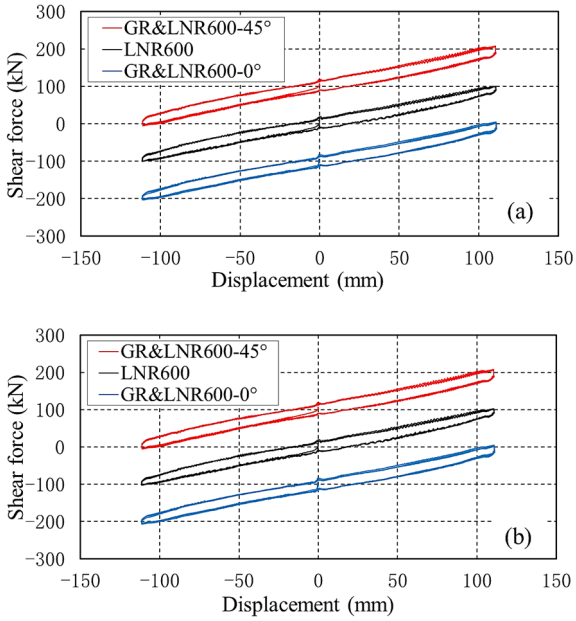


Figure 9. Hysteresis curves of horizontal shear tests: (**a**) compression–shear; (**b**) tensile–shear.

Table 3. Measured horizontal equivalent stiffness (K_b) in kN/mm.

Type	Compression–Shear	Tensile–Shear	Deviation
LNR600	0.891	0.927	4.1%
GR&LNR600-45°	0.927	0.960	3.6%
GR&LNR600-0°	0.926	0.957	3.4%

An analysis of Table 3 reveals that the horizontal equivalent stiffness of the specimens consistently demonstrates greater values under tensile–shear loading in comparison to compression–shear loading, albeit not exceeding 4.1%. Furthermore, the angle between the horizontal shear direction and the guide rail exhibits a certain enhancing effect on the horizontal equivalent stiffness, but within 4%. Consequently, it is concluded that the influence of GRs on the horizontal performance of rubber isolation bearings can be deemed negligible. In other words, the horizontal mechanical properties of the GRT&RB are akin to those of RBs of the same scale.

4. Numerical Analysis of Seismic Response

4.1. Building for Numerical Analysis

The building under investigation is a reinforced concrete high-rise shear wall structure characterized by an aspect ratio of 3.92. Its superstructure comprises 17 storeys, with a total height of 51 m. Specifics regarding the concrete properties are as follows: the compressive strength of the concrete for the first and second storeys is 26.8 MPa, featuring a wall thickness of 300 mm for the first level and 250 mm for the second storey. For the 3rd to 17th storeys, the compressive strength of the concrete is recorded as fc = 20.1 MPa, with a wall thickness ranging from 200 mm to 250 mm. Furthermore, the floor slab thickness for the first to fourth storeys measures 150 mm, while, for the 5th to 17th storeys, it is 120 mm.

The isolation system employed in this study encompasses a total of 24 rubber isolation bearings, inclusive of guided-rail tension-type rubber bearings and traditional rubber bearings. Additionally, a conventional isolation model (referred to as M_0) solely featuring traditional rubber bearings was established. To explore the impact of the elastic tensile stiffness and aperture on the tensile performance of GRs, nine comparative models with varying elastic tensile stiffness and aperture were devised. For ease of reference, the subscript in the model number denotes the specific elastic tensile stiffness and clearance. For instance, $M_{k(1.5)l(1)}$ signifies that the elastic tensile stiffness of the GR is 1.5 times the

test value, while the gap value is equivalent to the test value. Subsequent model numbers follow this sequence. The layout and dimensions of the structural plane and isolation layer are depicted in Figure 10.

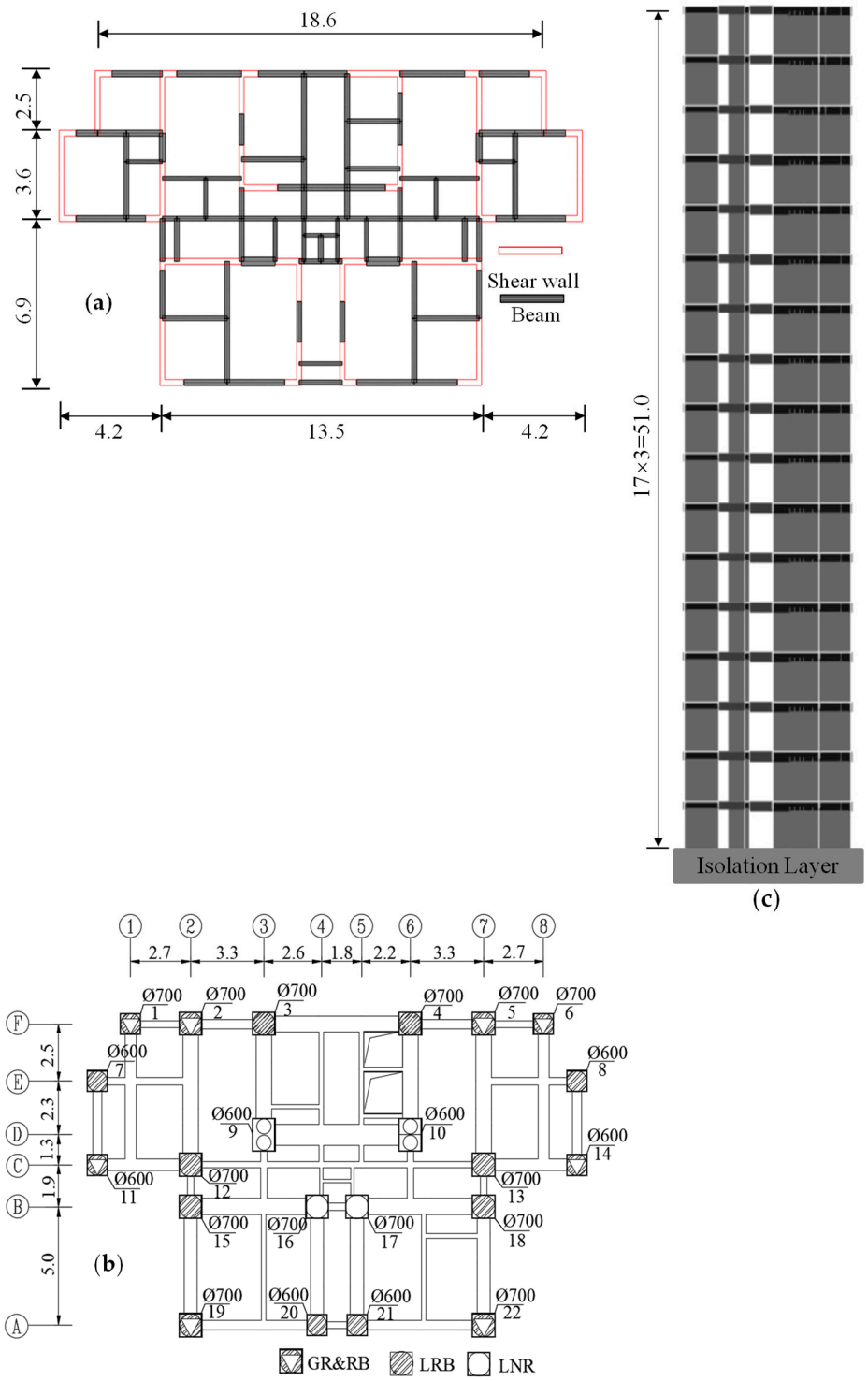


Figure 10. Model of high-rise shear wall building: (**a**) plan view; (**b**) layout of isolation layer; (**c**) elevation. Unit: m.

The mechanical properties of the GRs in each model are shown in Table 4.

Table 4. Mechanical properties of GRs.

Model No.	M_0	$M_{k(1)l(1)}$	$M_{k(2)l(1)}$	$M_{k(3)l(1)}$	$M_{k(1)l(0.5)}$	$M_{k(2)l(0.5)}$	$M_{k(3)l(0.5)}$	$M_{k(1)l(0)}$	$M_{k(2)l(0)}$	$M_{k(3)l(0)}$
Elastic tensile stiffness k (kN/mm)	/	27.6	55.2	82.8	27.6	55.2	82.8	27.6	55.2	82.8
Open l (mm)	/	1.4	1.4	1.4	0.7	0.7	0.7	0	0	0

Numerous empirical investigations have substantiated the nonlinearity exhibited by RBs in both horizontal and vertical orientations, commonly delineated by hysteresis loops. The analysis was executed utilizing the 2019 iteration of the ETABS software. The behavior of the RBs was simulated through the implementation of a hysteretic isolator, which amalgamated the attributes of axial elasticity and interconnected horizontal plasticity. The hysteretic isolator, illustrated in Figure 11, incorporates a plasticity model derived from the hysteresis characteristics introduced by Wen [30], Park, Wen, and Ang [31] and validated for base isolation evaluations by Nagarajaiah, Reinhorn, and Constantinou [32].

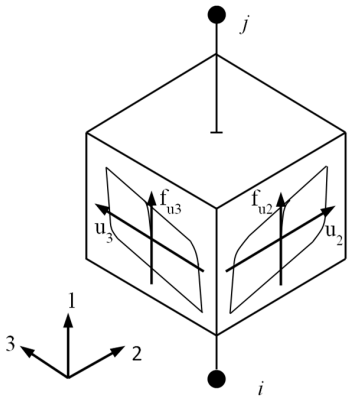


Figure 11. Hysteretic isolator horizontal property.

Although RBs exhibit nonlinear hysteretic behavior in the vertical direction, in this study, the tensile and compressive stiffnesses were modeled as linear to rapidly obtain relatively accurate results. Additionally, references [14,33] suggest that the vertical tensile stiffness of rubber bearings typically ranges from one fifth to one tenth of the compressive stiffness. This study simplifies both the compressive and tensile stiffness of RBs as linear to provide a relatively accurate portrayal of their vertical mechanical properties through the parallel combination of a hysteretic isolator and a gap. Furthermore, the vertical mechanical behavior of the GR&RB is characterized by the inclusion of a Hook element in parallel with the former. The models depicting the vertical mechanical behaviors of the RB and GR&RB are delineated in Figure 12.

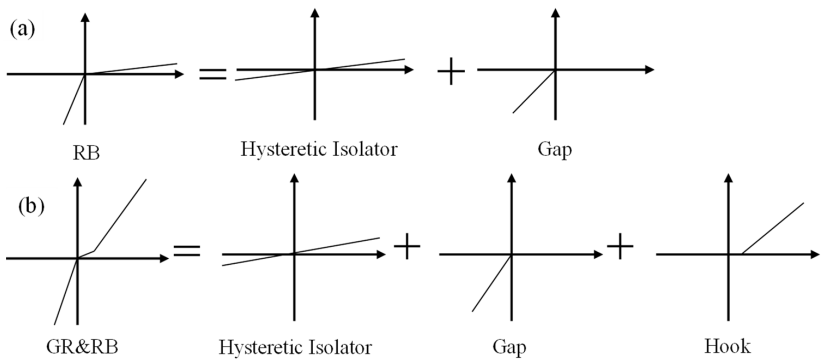


Figure 12. Vertical mechanical performance model: (**a**) RB; (**b**) GR&RB.

To enhance the precision and computational effectiveness, the horizontal and vertical mechanical hysteresis characteristics of RBs can be effectively replicated using the Vaiana–Rosati model (VRM) developed by Vaiana and Rosati [34,35].

Table 5 delineates the mechanical properties of the conventional rubber isolation bearings utilized in the numerical analysis conducted in this study.

Table 5. Mechanical properties of traditional rubber isolation bearings.

Type	Vertical Compressive Stiffness (kN/mm)	Vertical Tensile Stiffness (kN/mm)	Horizontal Equivalent Stiffness (kN/mm)	Initial Shear Stiffness (kN/mm)	Post-Yielding Stiffness (kN/mm)	Yield Strength (kN)
LNR600	1800	180	0.96	/	/	/
LRB600	2100	210	1.58	13.11	1.01	63
LNR700	2350	235	1.17	/	/	/
LRB700	2600	260	1.87	15.19	1.17	90

In consideration of the effective duration and the consistent soil type, the three-directional El Centro earthquake records, widely employed in seismic engineering research, were chosen for the nonlinear dynamic time history analysis. Given the focus of the present study on investigating the tensile performance and influencing factors of guided-rail-type tensile rubber bearings, the selection of a representative group of ground motions for excitation was sufficient. Figure 13 provides a depiction of the waveform of the El Centro earthquake.

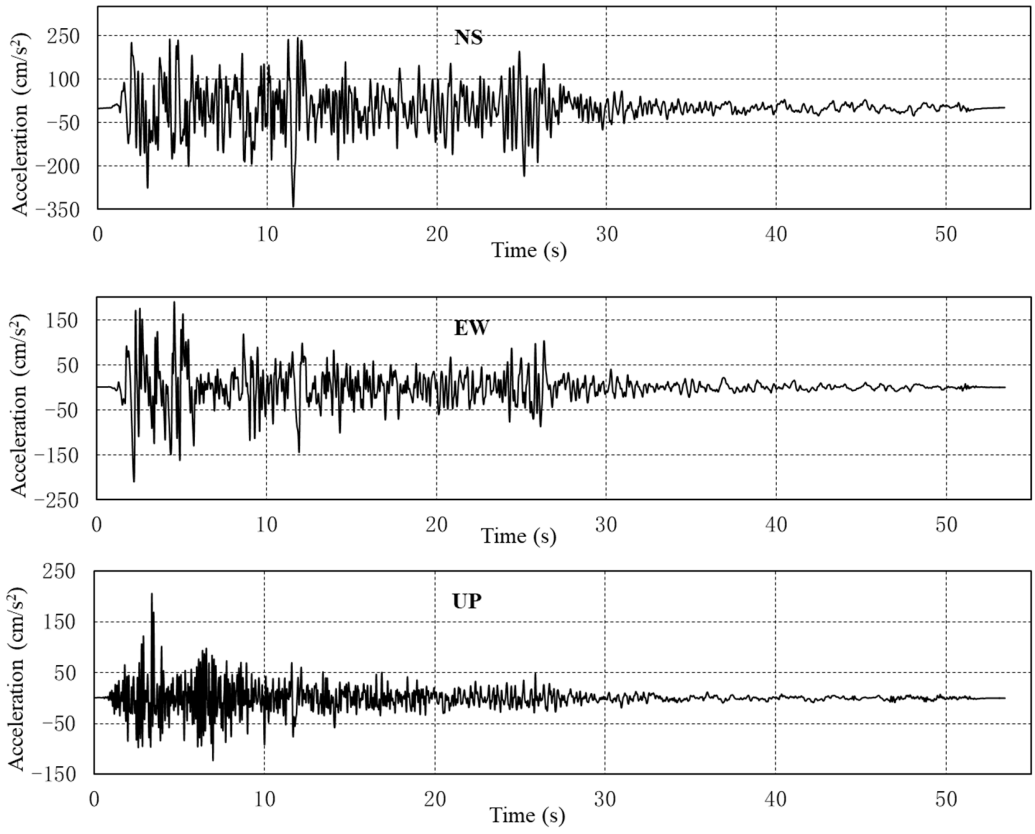


Figure 13. El Centro ground acceleration records.

The nonlinear time domain analysis method employed in ETABS incorporates material linearity and link nonlinearity. Furthermore, the analysis utilizes nonlinear direct integration through the Hilber–Hughes–Taylor alpha method [36].

4.2. Tensile Performance of Isolators

Figure 14 illustrates the vertical stress distribution of the rubber bearings under the El Centro seismic action for eight numerical models. The application of the GR&RB is observed to reduce the tensile stress level of the rubber isolators without altering the loading state of the rubber bearings, as evidenced in Figure 14. A comparison of the tensile effects depicted in Figure 14a,b suggests that the tensile effect is amplified with an increase in the elastic tensile stiffness of the GR, and it also escalates with a decrease in the open value of the GR.

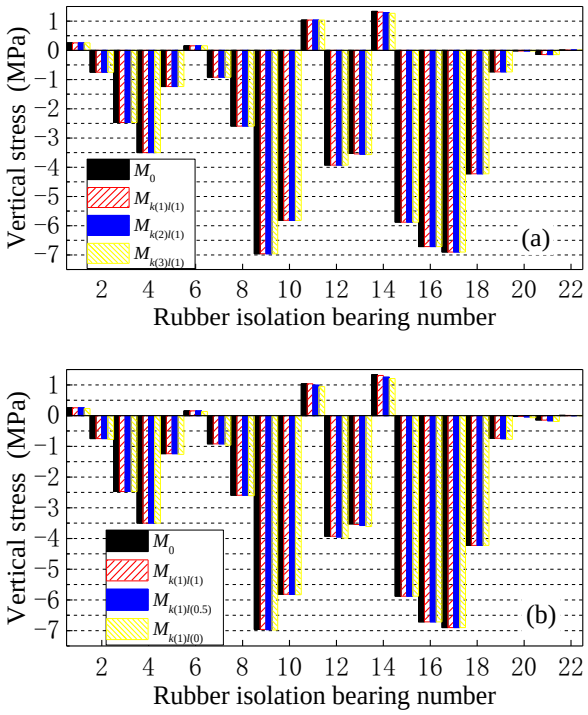


Figure 14. Vertical stress distribution: (**a**) keeping the open value unchanged while changing the elastic tensile stiffness, (**b**) keeping the elastic tensile stiffness unchanged while changing the open value.

Moreover, Figure 15 presents the vertical force–time history curves of the No. 14 rubber isolation bearing.

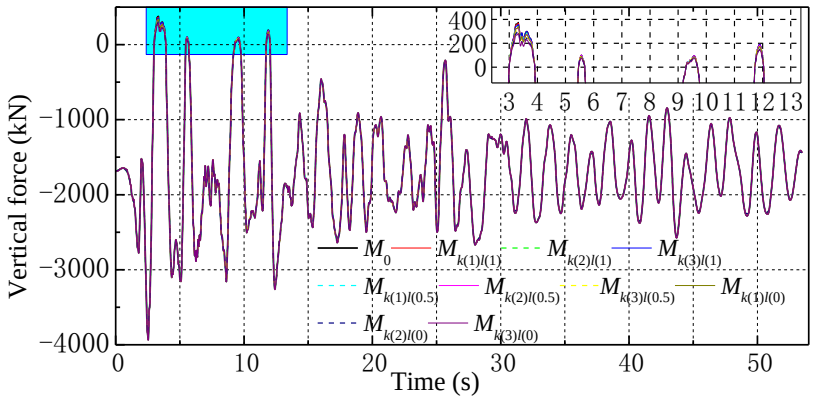


Figure 15. Vertical force–time history curves of No. 14 rubber isolation bearing.

As depicted in Figure 15, the activation of the GR occurs exclusively when the rubber isolation bearing is subjected to tension, functioning in conjunction with the rubber bearing to counteract the tensile forces. Nevertheless, the existence of an opening leads to a delayed

tensile response in the GR. It is noteworthy that the greater the magnitude of the opening, the more prominent the phenomenon of delayed tensile force becomes, leading to the reduced tensile resistance effect of the GR.

The tensile stress ratio can be used to characterize the tensile efficiency of isolated structures:

$$\eta = \frac{\sigma}{\sigma_0} \tag{2}$$

where η is the tensile efficiency, σ is the maximum tensile stress of the rubber bearing for the comparative models, and σ_0 is the maximum tensile stress of the rubber bearing for M_0. Figure 16 illustrates the impact of the varying elastic tensile stiffness and open values of GRs on the tensile efficiency.

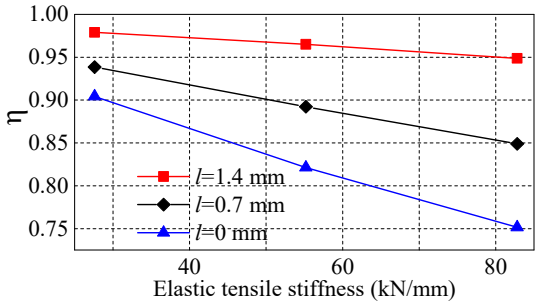


Figure 16. Tensile efficiency.

Based on the findings presented in Figure 16, the application of the GR&RB results in a reduction in tensile stress in the rubber isolation bearings by 75–98%. Optimal outcomes are achieved by enhancing the elastic tensile stiffness and concurrently reducing the open value of the GR, leading to a potential value of 75% tensile efficiency.

5. Conclusions

In order to mitigate the risk of overturning due to tension in rubber isolation bearings, a novel form of tensile rubber isolation bearing, denoted as the GR&RB, has been introduced. The mechanical characteristics of GRs, as well as the GR&LNR600 and LNR 600, have been thoroughly examined through quasi-static testing. Additionally, the impact of tensile efficiency factors such as the elastic tensile stiffness and the open value of the GR have been explored via finite element analysis. The key findings and implications derived from this investigation can be summarized as follows.

(1) The presence of clearance results in a slip stage during the initial phase of single GR stretching, thereby enabling the characterization of the GR's tensile behavior as Hook. Moreover, during finite element simulation, the vertical mechanical behavior of the GR&RB can be effectively represented through the parallel superposition of the hysteretic isolator, gap, and Hook.

(2) Within the elastic tensile range of rubber bearings, the tensile strength of the GR&RB is approximately 4.3 times greater than that of RBs of equivalent scale, underscoring the remarkable tensile capacity of the GR&RB.

(3) The horizontal mechanical performance of the GR&RB exhibits almost complete independence with respect to the angle of the guide rail and the loading direction, thereby equating the horizontal mechanical performance of the GR&RB to that of RBs of similar dimensions.

(4) The implementation of the GR&RB leads to a reduction in the level of tensile stress experienced by the rubber isolators. This reduction signifies that the utilization of the GR&RB diminishes the likelihood of failure related to overturning in seismic isolation structures by enhancing the tensile performance of the bearings. Furthermore, both an increase in the elastic tensile stiffness and a decrease in the open value of the GR can elevate the tensile strength of the GR&RB, with the optimal effect achieved through

an increase in the elastic tensile stiffness while simultaneously decreasing the open value of the GR.

Author Contributions: Investigation, L.Z., W.Y. and X.L.; methodology, L.Z. and W.Y.; formal analysis, L.Z. and K.W.; project administration, L.Z.; writing—original draft preparation, L.Z. and X.L.; writing—review and editing, L.Z. and K.W.; supervision, K.W.; funding acquisition, L.Z. All authors have read and agreed to the published version of the manuscript.

Funding: This research was funded by the general projects with joint special funds for basic research of Local Undergraduate Universities in Yunnan Province (Grant No. 202101BA070001-080 and 202101BA070001-176) and the Talent Introduction Project of Kunming University (Grant No. YJL20026).

Data Availability Statement: The data presented in this research are available upon request from the corresponding author.

Acknowledgments: The work presented in this paper has been supported by the Frontier Research Team of Kunming University 2023. The authors express their gratitude for the invaluable experimental support provided by the Kunming Earthquake Prevention and Disaster Reduction Technology Test Base, as well as for the provision of the experimental rubber isolation bearings by Yunnan GOWE Machinery & Technology Co., Ltd.

Conflicts of Interest: The authors declare no conflicts of interest.

References

1. Skinner, R.I.; Robinson, W.H.; Mcverry, G.H. *An Introduction to Seismic Isolation*; John Wiley & Sons, Inc.: New York, NY, USA, 1993.
2. Jin, J.M.; Tan, P.; Zhou, F.L.; Ma, Y.H.; Shen, C.Y. Shaking table test study on mid-story isolation structure. *Adv. Mater. Res.* **2012**, *446–449*, 378–381. [CrossRef]
3. Zheng, G.; Xu, H. Research on shaking table test of base and story isolation structures. *Appl. Mech. Mater.* **2014**, *580–583*, 1776–1781. [CrossRef]
4. Wu, Y.; Lu, J.; Qi, A. Shaking table test and numerical analysis of mid-story isolation eccentric structure with tower–podium. *Adv. Mech. Eng.* **2019**, *11*, 1687814018819562. [CrossRef]
5. Zhang, L.F.; Tao, Z.; Pan, W.; Wu, Z.J.; Lan, X. Shaking table test on isolated step-terrace frame structure in mountainous area. *J. Build. Struct.* **2020**, *41*, 24–32.
6. Rayegani, A.; Nouri, G. Application of smart dampers for prevention of seismic pounding in isolated structures subjected to near-fault earthquakes. *J. Earthq. Eng.* **2022**, *26*, 4069–4084. [CrossRef]
7. Rayegani, A.; Nouri, G. Seismic collapse probability and life cycle cost assessment of isolated structures subjected to pounding with smart hybrid isolation system using a modified fuzzy based controller. *Structures* **2022**, *44*, 30–41. [CrossRef]
8. Zelleke, D.H.; Saha, S.K.; Matsagar, V.A. Reliability-based multi-hazard design optimization of base-isolated buildings. *Eng. Struct.* **2024**, *301*, 117242. [CrossRef]
9. Tena-Colunga, A.; Parra-García, D.F. Seismic resilient performance of code-designed, base-isolated slender steel buildings in firm soils. *Structures* **2024**, *59*, 105754. [CrossRef]
10. Luo, Q.; Tan, Y.; Guo, M.; Pan, K.; Shang, Q.; Gao, G. Seismic isolation structural design for a 100-meter-high residential building of Tianhu Jingxiu Shantytown Renovation project in Kunming. *Build. Struct.* **2016**, *46*, 33–38.
11. *GB 50011-2010*; Code for Seismic Design of Buildings. China Architecture & Building Press: Beijing, China, 2016.
12. *GB/T 51408-2021*; Standard for Seismic Isolation Design of Buildings. China Architecture & Building Press: Beijing, China, 2021.
13. Zhou, F. *Engineering Structure Vibration Control*; Seismological Press: Beijing, China, 1997.
14. Architectural Institute of Japan. *Recommendation for the Design of Base Isolated Buildings*; Liu, W., Translator; Seismological Press: Beijing, China, 2006.
15. Kumar, M.; Whittaker, A.S.; Constantinou, M.C. Experimental investigation of cavitation in elastomeric seismic isolation bearings. *Eng. Struct.* **2015**, *101*, 290–305. [CrossRef]
16. Yang, Q.R.; Liu, W.G.; He, W.F.; Feng, D.M. Tensile stiffness and deformation model of rubber isolators in tension and tension-shear states. *J. Eng. Mech.* **2010**, *136*, 429–437. [CrossRef]
17. Cheng, H.; Liu, W.; Wang, S. Analysis of the tension of rubber bearings in the design of isolated high-rise buildings. *Earthq. Eng. Eng. Dyn.* **2007**, *27*, 161–166.
18. Kelly, J.M.; Griffith, M.C.; Aiken, I.D. *A Displacement Control and Uplift Restraint Device for Base Isolated Structures*; The Pacific Earthquake Engineering Research Center: Berkeley, CA, USA, 1987.
19. Nagarajaiah, S.; Reinhorn, A.M.; Constantinou, M.C. Experimental-study of sliding isolated structures with uplift restraint. *J. Struct. Eng.* **1992**, *118*, 1666–1682. [CrossRef]
20. Kasalanati, A.; Constantinou, M.C. Testing and modeling of prestressed isolators. *J. Struct. Eng.* **2005**, *131*, 857–866. [CrossRef]

21. Qi, A.; Lin, Y. Research on the approaches to incease the height-width ratio with supplemental steel bar. *Earthq. Eng. Eng. Vib.* **2005**, *46*, 33–38.
22. Yan, X.; Zhang, Y.; Wang, H. Experimental study on mechanical properties of three kind three-dimensional base isolation and overturn resistance devices. *J. Vib. Shock* **2009**, *28*, 49–53.
23. Su, J.; Heisha, W.L.H.; Zhou, F. Study on an innovation tensile-resistant device for laminated rubber bearing. *Ind. Constr.* **2010**, *40*, 43–46.
24. Wang, D.; Lu, X. Experimental research on mechanical properties of anti-tension isolation bearing. *J. Build. Struct.* **2015**, *36*, 124–132.
25. Ge, J.; Zhang, L.; Zhang, G.; Liu, X.; Ma, B.; Guan, Z. Study on design of tensile base performance of the Chengdu museum isolation structure. *J. Build. Struct.* **2016**, *37*, 16–23.
26. Pauletta, M.; Pinzano, F.; Frappa, G.; Russo, G. Tensile tests for the improvement of adhesion between rubber and steel layers in elastomeric isolators. *Appl. Sci.* **2020**, *10*, 8063. [CrossRef]
27. Zhang, Z.; Vassiliou, M.F.; Zhou, Y. Numerical and analytical investigations on tensile behavior of thick rubber bearings. *Eng. Struct.* **2024**, *301*, 117313. [CrossRef]
28. Vaiana, N.; Sessa, S.; Marmo, F.; Rosati, L. An accurate and computationally efficient uniaxial phenomenological model for steel and fiber reinforced elastomeric bearings. *Compos. Struct.* **2019**, *211*, 196–212. [CrossRef]
29. *JGT 118-2018*; Rubber Isolation Bearings for Buildings. Standards Press of China: Beijing, China, 2018.
30. Wen, Y.K. Method for random vibration of hysteretic systems. *J. Eng. Mech.* **1976**, *102*, 249–263. [CrossRef]
31. Park, Y.J.; Wen, Y.K.; Ang, A.H.S. *Earthquake-Resistant Design of Building Structures*; CRC Press: Boca Raton, FL, USA, 1986.
32. Nagarajaiah, S.; Reinhorn, A.M.; Constantinou, M.C. A simplified method for base isolation system design. *Earthq. Eng. Struct. Dyn.* **1991**, *20*, 371–391.
33. Wu, R.; Wang, S.; Liu, W.; Du, D. Research on influence of difference between pulling and pushing stiffness of RB&LRB upon the isolation effectiveness. *Earthq. Resist. Eng. Retrofit.* **2008**, *30*, 24–28.
34. Vaiana, N.; Rosati, L. Classification and unified phenomenological modeling of complex uniaxial rate-independent hysteretic responses. *Mech. Syst. Signal Process.* **2023**, *182*, 109539. [CrossRef]
35. Vaiana, N.; Rosati, L. Analytical and differential reformulations of the Vaiana–Rosati model for complex rate-independent mechanical hysteresis phenomena. *Mech. Syst. Signal Process.* **2023**, *199*, 110448. [CrossRef]
36. Wilson, E. *Three-dimensional Static and Dynamic Analysis of Structures*; Computers & Structures Inc.: Berkeley, CA, USA, 2002.

Disclaimer/Publisher's Note: The statements, opinions and data contained in all publications are solely those of the individual author(s) and contributor(s) and not of MDPI and/or the editor(s). MDPI and/or the editor(s) disclaim responsibility for any injury to people or property resulting from any ideas, methods, instructions or products referred to in the content.